Towards a single-molecule FRET study of Frauenfelder's nonexponential rebinding of CO in myoglobin

Eskandari Alughare, Z.

Citation
Eskandari Alughare, Z. (2022, June 23). *Towards a single-molecule FRET study of Frauenfelder's nonexponential rebinding of CO in myoglobin. Casimir PhD Series*. Retrieved from https://hdl.handle.net/1887/3348505

2

The photodissociation of carboxymyoglobin (MbCO)

This chapter focuses on myoglobin, a relatively small protein (~18 kDa) which is present in all vertebrate systems. Myoglobin plays an essential role in the diffusion of oxygen to the mitochondria of aerobic muscle, and also as oxygen storage for metabolic respiration during periods of hypoxia or high oxygen demand. This chapter presents an introduction with special focus on myoglobin characterization and on the kinetics of the rebinding reaction of a CO molecule after photodissociation.

2.1 Myoglobin function

Myoglobin is a single-subunit intercellular protein found in vertebrates particularly in mammals. [2] Its main function is to deliver oxygen to the mitochondria in red muscle cells. [1,3] Similarly to hemoglobin (Hb), myoglobin (Mb) is a heme protein whose physiological importance is principally related to its ability to bind molecular oxygen via its heme cofactor. Its structure is similar to the subunits of hemoglobin and although the heme cofactor is identical in both of them, myoglobin has higher oxygen binding affinity than hemoglobin: In the blood of a healthy person, the partial pressure of oxygen (pO_2) for Hb is approximately 26 mm Hg at 50% saturation of Hb. However, pO_2 for Mb for this condition is about 1 mm Hg. [4] This difference in affinity leads to these proteins performing different functions in the body. [5] Whereas hemoglobin is responsible for binding oxygen in the lung and transporting the bound oxygen through the body via the bloodstream, myoglobin is found mostly in muscle tissue as an intracellular storage site for oxygen. [6]

Like oxygen, carbon monoxide binds coordinately to the heme's iron atom, but its binding affinity is 240 times greater than that of oxygen. This preferential binding of carbon monoxide is largely responsible for the asphyxiation resulting from carbon monoxide poisoning: [7] CO replaces oxygen in hemoglobin, decreasing the oxygen-carrying capacity and resulting in less released oxygen to tissues. [8] Similarly, CO when bound to myoglobin, leads to a lower supply of oxygen to the muscles. [9] Other heme-containing proteins, in particular mitochondrial cytochrome c oxidase, can also be a target site in human acute CO poisoning. [10] For more than a hundred years, carbon monoxide (CO) has been known as a toxic-killer substance that competes with oxygen for delivery to tissues. In recent years, it has been discovered that low concentrations of CO show remarkable protective effects as a cytoprotective and homeostatic molecule with important signaling capabilities and pathophysiological situation. [11] Moreover, each cell of a mammalian organism expresses heme oxygenase enzymes for continuous generation of CO with a key role in circadian rhythms, memory and hemodynamic regulation. [12,13]

2.2 Myoglobin structure

Myoglobin was the first protein that its three-dimensional structure determined by X-ray crystallography. This crystal structure was revealed by J.C. Kendrew, who shared the 1962 Nobel Prize in chemistry with Max Perutz [14] for this work. Myoglobin with a molecular mass of 18 kDa is a monomeric protein consisting of seven α-helical and six non-helical segments, which contains 153 amino acids [15] that form a binding pocket for the heme cofactor to be discussed below (Figure 2.1A).

The iron ion has six positions to bind ligands, four of which are provided by the nitrogen atoms of the four pyroles of a porphyrin. The π electron system of the porphyrin interacts with an iron d-orbital in the porphyrin plane. The imidazole side chain of His93 (proximal histidine) is attached directly to the iron (Figure 2.1B). It provides the fifth ligand, stabilizing the heme group and slightly displacing the iron ion away from the plane of the heme. The sixth ligand position is available for potential ligands such as O_2, CO or NO. His-64 (distal histidine) interacts with ligand substrates but not with iron. These two main interactions between the heme's iron center, the porphyrin ring and the surrounding amino acids stabilize the heme–protein conjugate.
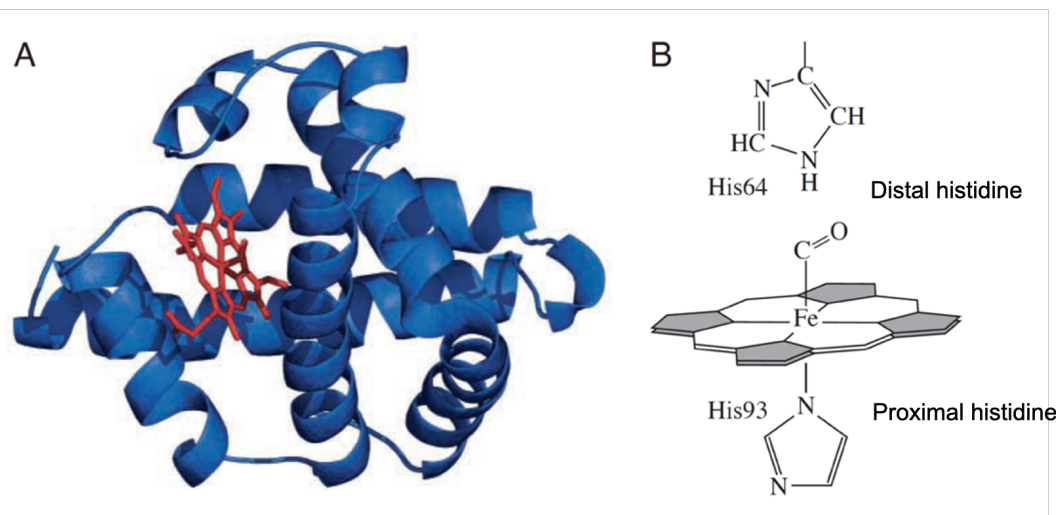
Figure 2.1. *(A) The myoglobin structure consists of eight α-helices (blue) that surround a central heme pocket (red). The heme binds to various gaseous ligands including oxygen, carbon monoxide and nitric oxide. (B) The protoheme group is stabilized by two histidine amino acids: the distal histidine residue above (His64) and the proximal histidine below (His93).* [15]

The porphyrin group is a heterocyclic organic macrocycle, consisting of four modified pyrrole rings joined by methine bridges (=CH−). The core structure of porphyrin is called porphin (Figure 2A). [16,17] Typical absorption spectra of porphyrins exhibit two main features, a single intense band named the Soret band and a group of weaker bands called Q-bands (Figure 2.2B). [18]
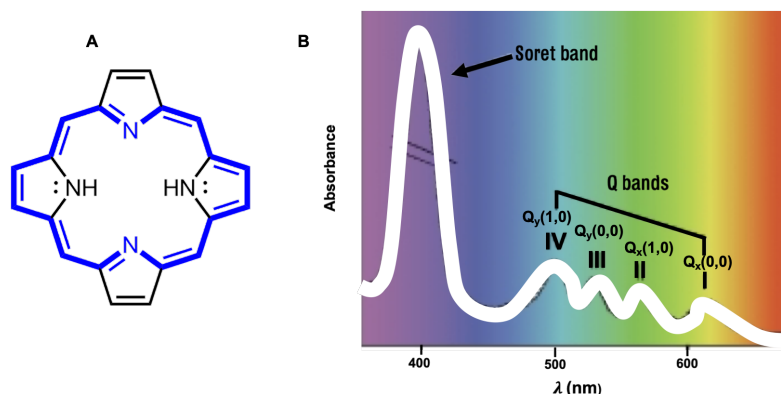

Figure 2.2 *(A) The chemical structure of porphin and (B) The absorption spectra of porphyrin. The strong peak is referred to as the Soret band and the weak group appearing at higher wavelength is split into four bands.* [17,19]

There are three relevant ligation states for myoglobin, metmyoglobin (met-Mb), in which the iron is in the oxidized form (Fe^{3+}) and a water molecule is covalently bound to the heme; deoxymyoglobin (deoxy-Mb), in which the iron is in the ferrous state (Fe^{2+}) and no ligand is bound to the iron, leaving it with an unoccupied sixth coordination site; and oxymyoglobin (oxy-Mb) or carboxymyoglobin (MbCO), in which the iron is in the ferrous state (Fe^{+2}) and has a ligand (O_2 or CO) covalently bound to the heme via the iron's sixth coordination site. [20]

These different oxidation states of iron and the type of bound ligand can be readily identified using ultra-violet/visible (Uv-vis) absorption spectra (Figure 2.3). The main

features of the Mb Uv-Vis spectra stem from the heme cofactor and consist of (1) the Soret-band in the 365 to 500 nm region and (2) the Q-bands in the 500 to 700 nm region. For met-Mb, the Soret band peak appears at 409 nm and the Q-band is marked by a weak peak at around 503 nm (Figure 2.3A, brown color) while, in deoxymyoglobin (deoxy-Mb), the Soret peak is observed at 433 nm and the Q-band shows a strong peak at 555 nm (Figure 2.3B, green color). Binding of CO (carbonoxymyoglobin, MbCO) shifts the Soret band to 423 nm and splits the Q-band into two peaks centered at 540 nm and 580 nm (Figure 2.3C, red color). Figure 2.4 shows the difference between deoxy-Mb and MbCO states in the Q-bands (500-700 nm) (Figure 2.4A), and Near-Infrared (NIR) (700-1000 nm) regions of the spectrum (Figure 2.4B). [20,21]
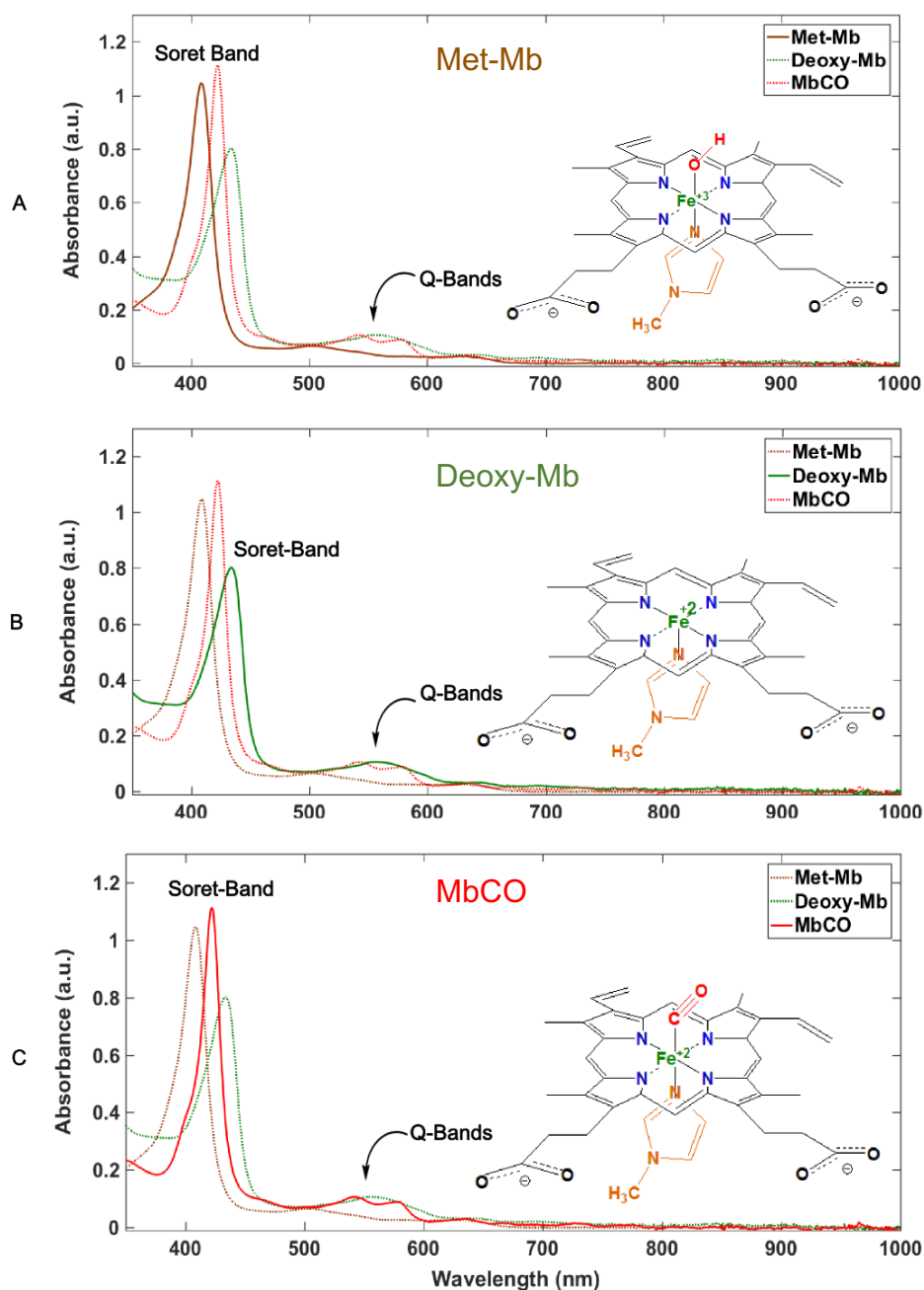
Figure 2.3. *Absorption spectra and chemical structures of heme for met-Mb (A), deoxy-Mb (B), and MbCO (C). All absorption spectra have been measured experimentally at Leiden University.*
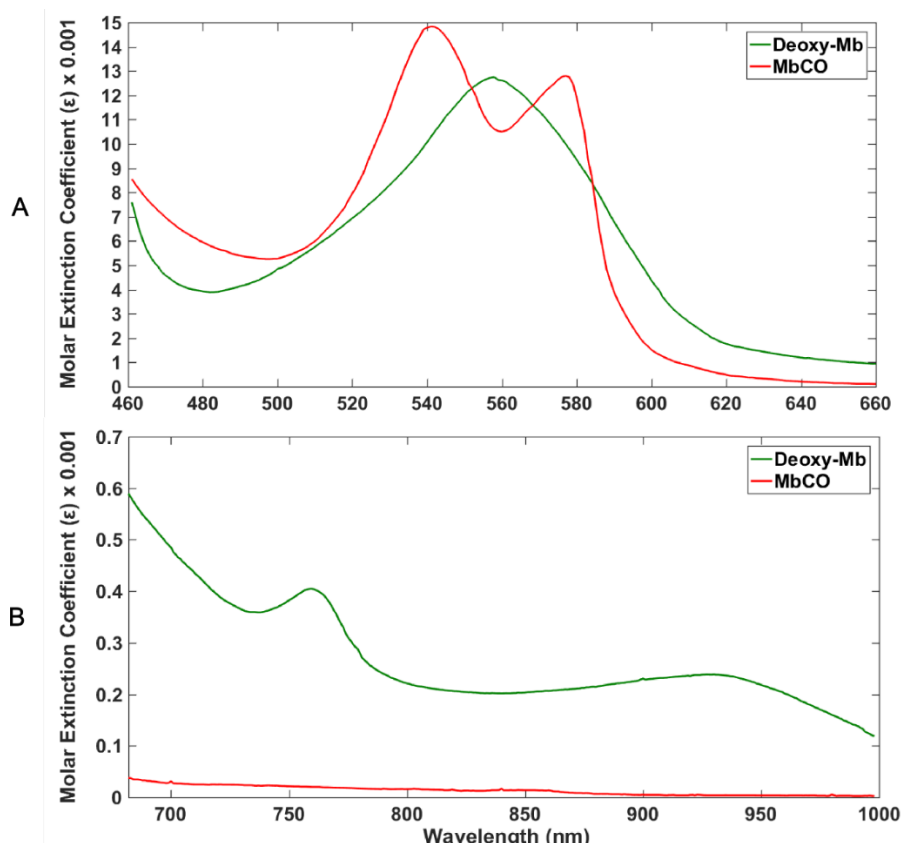
Figure 2.4. *(A) A comparison of the Q-bands (500-700 nm) and (B) NIR (700-1000 nm) bands between deoxy-Mb and MbCO.* [21]

2.3 Components of MbCO and deoxy-Mb spectra

As discussed above, association or dissociation of ligands to the heme is accompanied by spectral changes in the visible, infrared, and ultraviolet regions of the spectrum and by modifications of the magnetochemical features. This section will discuss in more detail which transitions these features stem from and how they relate to the structural changes due to ligand binding.

2.3.1 Soret Band

The main electronic transitions are related to the π electron system of the porphyrin ring, the d-orbitals of the iron atom and the nearby proximal Histidine. They comprise the intense band around 400 nm named the Soret band and the lowest-energy visible band around 550 nm.

The spectrum of Mb in the Soret region consists of a single band, which is attributed to a porphyrin $\pi \rightarrow \pi^*$ electronic transition. Based on the Gouterman's theory of the origin of absorption bands in a porphyrin system, HOMOs (Highest Occupied Molecular Orbitals) are formed by two nearly degenerate a_{1u} and a_{2u} orbitals and the LUMOs (Lowest Unoccupied Molecular Orbitals) are formed by a set of e_g orbitals (Figure 2.5A). Transitions between these orbitals lead to two excited states of ^1E_u character. The Soret band arises from excitation from the two orbitals $a_{1u}(\pi)$ and $a_{2u}(\pi)$ to the higher energy E_u orbitals of the porphyrin ring (Figure 2.5B). [22,23]
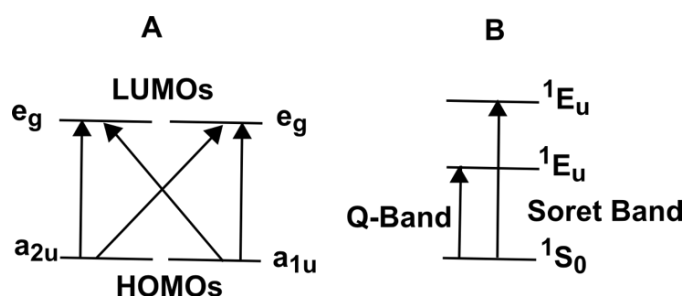
Figure 2.5. (A) Gouterman's model; a_{1u} and a_{2u} orbitals (HOMOs) and the two e_g orbitals (LUMOs), (B) Energy levels and electronic transitions of Soret band and Q-band in porphyrins. [22]

2.3.2 Q- Band

There is another porphyrin $\pi \rightarrow \pi^*$ electronic transition at the lower energy side of the two bands usually denoted by [Q(0,0) and Q(1,0)]. In a symmetric molecule, the first excited state, S_1, is a degenerate state comprising Q_x and Q_y components. At lower symmetry, the above-mentioned bands are further split into two bands each. The X and Y components are no longer degenerate and therefore we see four bands in the Q band region, which are denoted by Qx(0,0), Qy(0,0), Qx(1,0) and Qy(1,0) (Figure 2.2B). [23] These four bands in the visible regions of the spectrum are allowed by D_2 symmetry. In case of a metalloporphyrin, the symmetry changes from D_2 to D_{4h} because the two of the inner pyrrole hydrogens are replaced by metal-nitrogen bonds. Thus, the coplanar metalloporphyrins have a higher symmetry. [24,25] The lack of two hydrogens reduces the number of visible bands from four group bands (Figure 2.2B) to two group bands, such as in myoglobin (Figure 2.3).

2.3.3 Near Infrared

The NIR (750- 2500 nm) regions of the spectrum of deoxy-Mb exhibits three bands that are labeled I, II, and III (Figure 2.6B). Band I is related to a charge-transfer from the iron to the porphyrin [$d_{xz} \rightarrow e_g(\pi^*)$)], band II corresponds to an iron d→d transition ($d_{xz} \rightarrow d_z{}^2$), and band III corresponds to a porphyrin to iron charge-transfer transition (a_{2u} (π) $\rightarrow d_{yz}$) (Figure 2.6A, green). Experimentally measuring band III is difficult due to its small extinction coefficient (approximately 350 M^{-1} cm^{-1}) at room temperature (Figure 2.6B). [26]

The transitions observed in the MbCO spectrum are classified in three types: 1) metal centered (d)→(d) transitions, 2) charge-transfer transitions from porphyrin to iron [(π) →(d)] and 3) promotions of an electron from either an iron d or porphin (π) orbital into the CO (π^*) orbital. [27] The optical spectrum of carboxymyoglobin is very much like that of a closed-shell metal porphyrin, which generally only exhibits the porphyrin Soret and Q bands (Figure 2.3C).

MbCO has a much lower extinction coefficient around 700-800 nm, (ε < 30 M^{-1} cm^{-1}) compared to deoxy-Mb (350 M^{-1} cm^{-1}) (Figure 2.6B), [28] but there is no evidence for NIR bands in either the crystal or solution absorption spectra of MbCO. [29,30] This lack of any near-infrared electronic absorption is important for the design of our experiments. The magnetic circular dichroism (MCD) technique can detect weak transitions which cannot be seen in an absorption spectrum. A near-ultraviolet-visible

MCD study of MbCO by Vickery et al. also provides no evidence for additional transitions. [20] The single-crystal data shown the absence of iron (d) →porphin (π*) transitions since there is no evidence for any z-polarized intensity as would be expected for the $d_{yz} \rightarrow e_g$ (π*) transitions. The most plausible assignment for bands I and II, then, is that they correspond to iron d → d transitions, as originally suggested by Eaton and Charney on the basis of their relatively large CD anisotropy factors. [31]
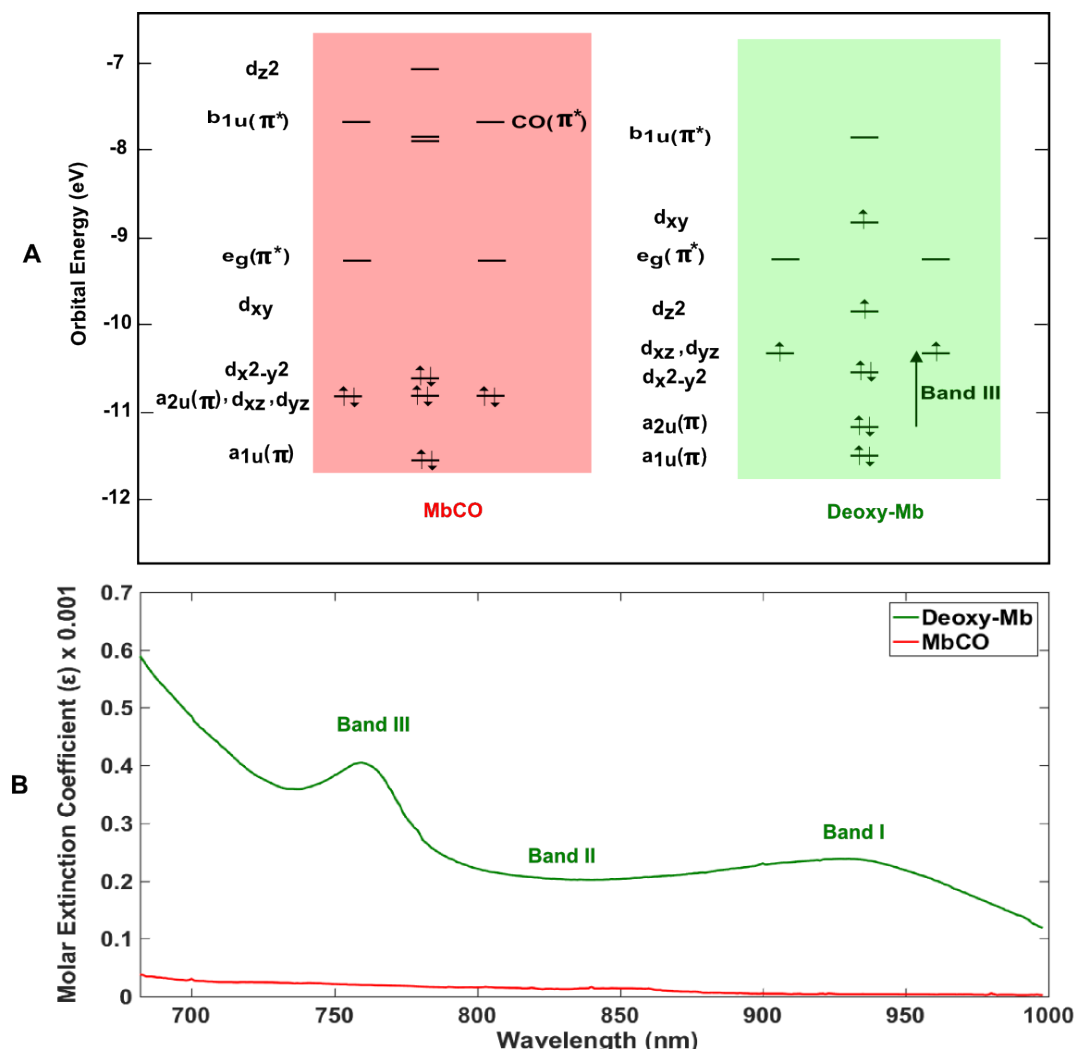
Figure 2.6. *(A) Extended Hückel orbital energies for MbCO (red), and deoxy-Mb (green). The arrow indicate the electronic transition related to Band III in deoxy-Mb (modified after [20]). (B) Comparison of the absorption in NIR region (700-1000 nm) between MbCO and deoxy-Mb. Band I, Band II, and Band III have been labeled for deoxy-Mb (modified after [21]).*

2.4 Photodissociation and its mechanism

Photodissociation and binding-rebinding rates provide useful information about conformational changes of myoglobin related to ligand migration inside protein pocket. Studies on the rebinding reaction rate of myoglobin with ligands have revealed a complex ligand-protein interaction after bond breaking, which results in multiple kinetic intermediates due to the protein relaxation and movements of the ligand within the protein. [32–35]
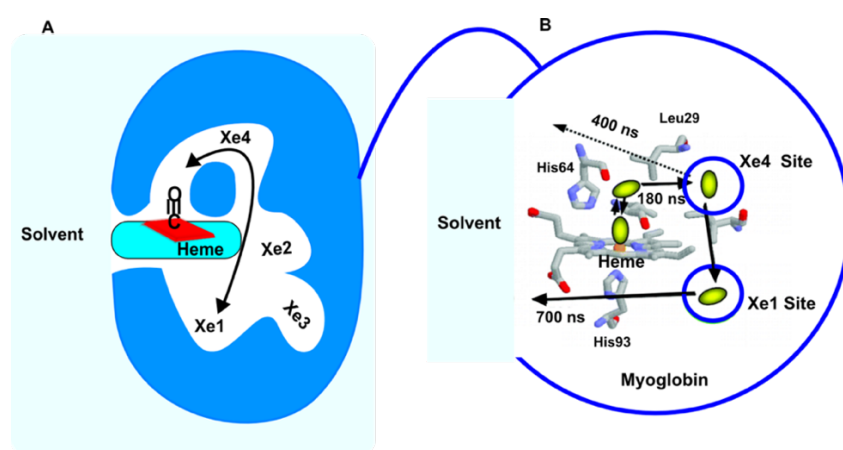
2.5 Photodissociation of Mb-CO bond

Over decades, many investigations have revealed that the carbon monoxide complex of myoglobin (MbCO) is light-sensitive. [36–38] Upon the absorption of a photon, the iron-carbon monoxide bond breaks (dissociation), and a series of spectroscopic and structural changes starts, after which the carbon monoxide spontaneously rebinds at room temperature and MbCO is reconstituted (recombination). [39–42] The dissociation and recombination reactions of Mb*CO have been investigated with various spectroscopic techniques at various temperatures and in a number of solvents. [43–51]

After photodissociation, the CO ligand is still located close to the heme (primary docking site) in the initial intermediate noted Mb:CO. From there, CO can either rebind again to the heme by crossing the inner barrier (geminate rebinding) or escape. In the latter case, CO migrates through the protein matrix to a different protein internal cavity, one of the so-called xenon cavities (Figure 2.7).

Figure 2.7A shows four internal cavities in myoglobin named Xe1, Xe2, Xe3, Xe4 that bind a xenon atom with high affinity (Figure 2.7A). [52] The extent of 'geminate' (internal) recombination from these sites depends on the reactivity of the ligand with the heme iron and on its ability to diffuse away from the active site to the xenon cavities.

Based on X-ray crystallography, it is found that CO accumulates in one of the Xe binding cavities (Xe1) which is located on the proximal side of the heme (the side in which the imidazole side chain of His93 is attached directly to the iron) (Figure 2.7A). The Xe1 site is highly occupied by the CO ligand and is the one with the highest affinity. The Xe4 pocket is another possible secondary binding site in the back of the distal pocket, located in the neighborhood of the primary docking site. According to MD simulations native MbCO, CO occupies the Xe4 cavity, which suggests a migration route from Xe4 to Xe1. [53,54]

From Xe(4), CO escapes to the solvent with a lifetime of 400 ns, but the transfer of CO to the Xe(1) trapping site occurs much faster. Thus, CO is trapped in the Xe(1) site and, from there, it escapes to the solvent with a lifetime of 700 ns. The docking positions of CO in wild type Mb: the primary docking site, Xe(4), and the Xe(1) sites, and the escape path of CO to the solvent are shown in Figure 2.7B. [55]

Figure 2.7. *(A) Schematic illustration of the internal xenon cavities in MbCO which consist of locations Xe1, Xe2, Xe3, Xe4 (modified after [56]). (B) Mechanism after Wild-type MbCO photodissociation at room temperature, which consists the geminate rebinding of CO ligand (green ellipsoid ball) with heme, migration to xenon cavities (Xe4, and Xe1), and escape to the solvent (modified after ref. [55]).*

As far as the photolytic state is concerned, the most widely accepted hypothesis is that dissociation occurs from a metal-to-ligand charge-transfer (MLCT) state.
Based on the experimental data, the fast heme dissociation step is not just one quick step; it is a complicated process which consists of several internal conversion (IC) steps along a series of intermediate excited states with gradual structural changes until it ends in the ground state of high spin deoxy-Mb (Figure 2.8). [42]
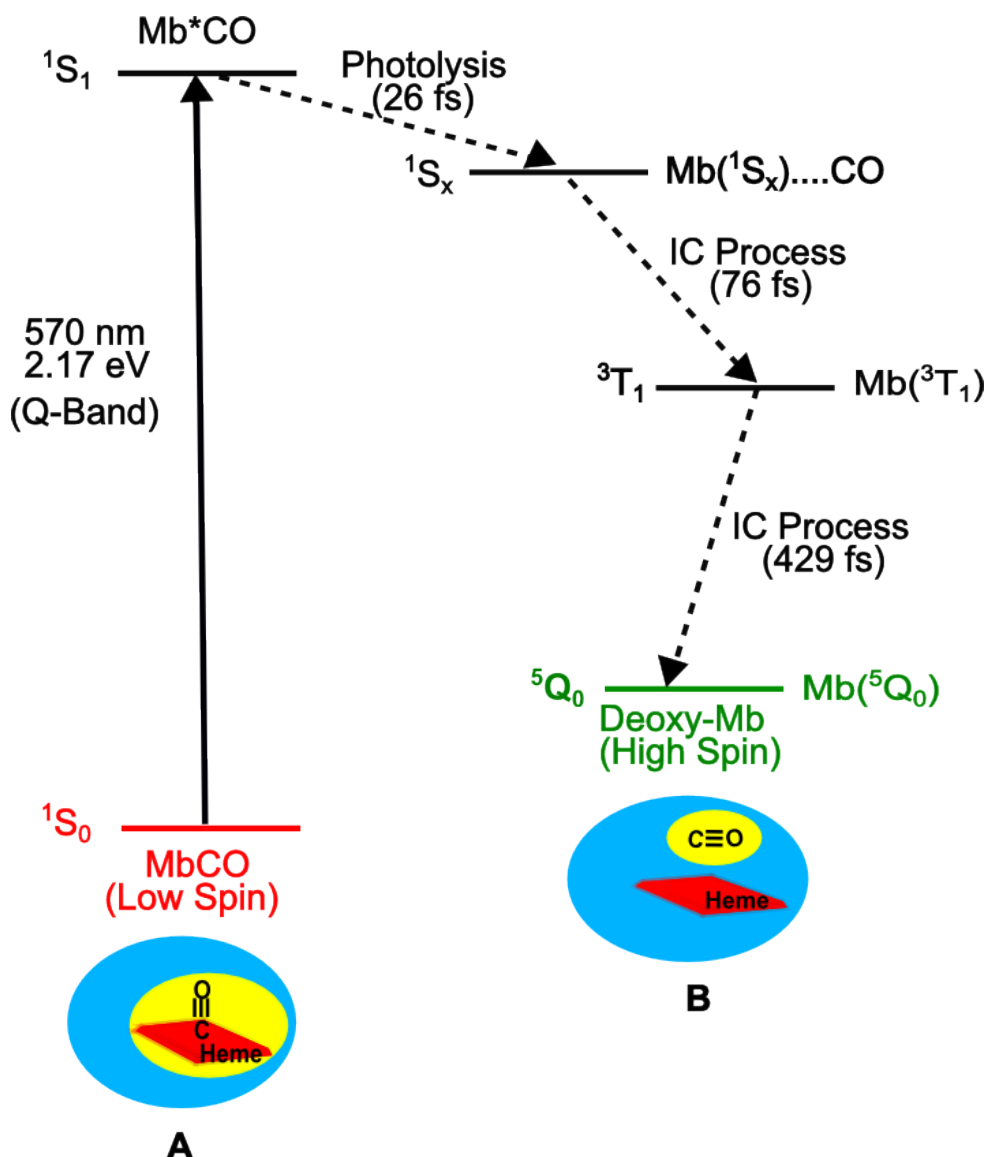
Figure 2.8. An energy level schematic for photodissociation of MbCO at room temperature. Illumination of MbCO at 570 nm and excitation from ground state ($^1S_0$) of MbCO (A) to the excited state ($^1S_1$), is followed by photodissociation within 50 fs to the first excited intermediate state (^1S_x) relaxes, through an IC process to the second intermediate excited state ($^3T_1$), and finally, through another IC process, the photodissociation completes and MbCO relaxes to the deoxy-Mb ground state ($^5Q_0$) (B) (modified after [42]).

This overall process encompasses three main sequential steps (Figure 2.8): [57] $^1S_1 \rightarrow {}^1MLCT \rightarrow {}^3MLCT \rightarrow {}^5MLCT$:
1). $^1S_1 \rightarrow {}^1S_x$ (^1MLCT): singlet lowest excited state to singlet metal-ligand CT state;

2). ^1S_x (^{1}MLCT) → $^3T_1$ (^{3}MLCT): spin crossover (ISC) from singlet metal-ligand CT state to triplet metal CT state;

3). $^3T_1$ (^{3}MLCT) → $^5Q_0$ (^{5}MLCT): spin crossover (ISC) from triplet metal-ligand CT state to quintet metal- ligand CT state;

The first relaxation step is a transition from the $^1S_1$ state of Mb*CO to a ^1S_x state of Mb….CO (*^{1}MLCT). This leads to a complete decay of the $^1S_1$ population after ~100 fs and the dissociation takes 26 fs (Figure 2.7A). Franzen et al. were the first to rule out the involvement of a high spin state in the transition from the Q state to a ^{1}MLCT state and they assigned a mechanism for the photolysis which was not considered before: the removal of one sigma bonding electron from an iron-CO (d_{Fe}- π_{CO}) orbital reduces the back-bonding of the CO ligand to the iron (d_{Fe}- π^*_{CO}). [57] The similarities of the excited states lifetimes and absorption maxima in the spectra of both ligated and unligated forms indicate that the first fast step already results in the dissociation of the ligand. Based on the proposed photophysical pathway, iron-to-ring charge-transfer is the key event in the mechanism of photolysis of diatomic ligands following a porphyrin ring π→π* transition.

The second step includes a change in the spin state of the Mb from a singlet (^1S_x) to a triplet ($^3T_1$, ^{3}MLCT) on a time scale of around 76 fs. This is followed by the third step in which the system relaxes to the deoxy-Mb with high-spin quintet state ($^5Q_0$, ^{5}MLCT) on a time scale of around 429 fs (Figure 2.7).

Basically, in MbCO, the iron atom is located within the plane of the porphyrin ring in a low spin state whereas, in deoxy-Mb, iron is about 0.3 Å out of the plane in a high-spin state. Experimental evolution of the Fe–C(O) distance and data obtained from the Fe out-of-plane distance also show that the iron goes out of the plane of the porphyrin ring almost instantly upon photodissociation and oscillates with a large amplitude with a 40 fs period. Therefore, this measured iron motion is probably due to crossover spin state where the iron switches from the low-spin configuration in the ligated species to of the unligated form. [57] Figure 2.9 shows the Fe out-of-plane upon photodissocation of MbCO and as it can be seen, the Fe–CO distance oscillates between the equilibrium distance (1.7–1.8 Å) (undissociated Mb-CO) and 2.5 Å (dissociated Mb-CO) (). The amplitude of the oscillation is initially 0.9 Å and reaches a value of 2.2 Å where CO is dissociated. Followed by initial oscillation, the wave packet is in the MLCT bands where, due to repulsive interactions, CO does not recombine to heme and continues oscillations. Relaxation of the structure restrains these oscillations to reach the equilibrium value of 2.2 Å. [57]
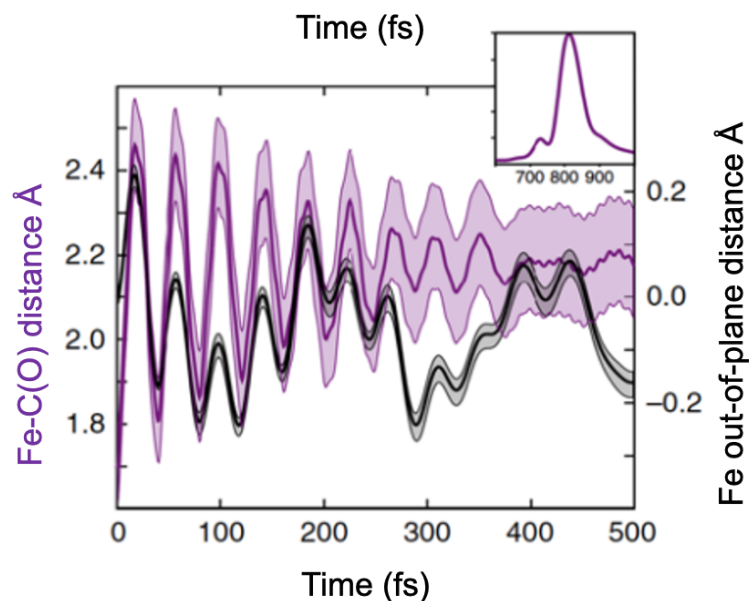
Figure 2.9. *Evolution of the Fe–C(O) distance (magenta, left axis) and of the Fe out-of-plane distance (black, right axis) upon photodissocation of MbCO. The amplitude of the oscillation is initially 0.9 Å. The Fe distance (Fe–C(O)) stabilizes at a value of 2.2 Å. At this distance, the CO is essentially photodissociated. The measured equilibrium distance of Fe–C(O) is between (1.7–1.8 Å) and 2.5 Å and the standard deviation of these geometric values is indicated by the shaded area. The Fourier transform of the Fe–C(O) oscillations is illustrated in the insert (in cm^{-1}).* [57]

Photodissociation of MbCO through excitation to the lowest excited state of the heme ($^1S_1$ of Mb*CO, Figure 2.7) is forced by a iron to porphyrin charge-transfer with a quantum yield of essentially 1. MCD studies have shown the lack of any near-infrared electronic absorption for MbCO. Also, the single-crystal data confirm the absence of a iron (d) —porphyrin (π*) transition since there is no evidence for any z-polarized intensity as would be expected for a d_{xz}, $d_{yz} \rightarrow$ ($e_g\pi^*$) transition. In the absorption spectrum of MbCO, there is a very-low-intensity absorption between 700-800 nm ($\varepsilon < 30$ M^{-1} cm^{-1}), which is not due to the metal to protein charge-transfer and may derive from a metal-centered iron (d) →(d) transition. Therefore, excitation of MbCO in the NIR is unlikely to facilitate photodissociation of MbCO. [20,27–29]

Many authors have studied the kinetics of rebinding after photodissociation and found that the rebinding parameters significantly change with temperature, solvent composition, viscosity, and the myoglobin mutant. [43–51,58–64]

Despite much work, [65–68] the ligand migration pathway and protein dynamics are still mysterious and not yet completely known. Frauenfelder has suggested that ligand binding is governed by successive barriers depending differently on temperature, and solvent. [69–72] Information regarding the barriers and the energy of the intermediates is very important to reach a coherent description of the dynamics of ligand binding to Mb, but our knowledge in this area is very limited.

Regarding the MbCO photodissociation at low temperature, several kinetic intermediates have been shown during geminate rebinding and recombination of the escaped ligand with the protein. However, at ambient temperature kinetics studies of MbCO photodissociation in water revealed no features of the multiple intermediate states except for geminate recombination kinetics. [73–77]

2.6 Photodissociation and CO rebinding at room temperature

In solution at physiological temperatures, a protein undergoes some conformational fluctuations that grow in related amplitude with temperature. In the case of MbCO, temperature enhancement facilitates ligand escape to the solution. [78]

Photodissociation in solution has been intensively investigated by measurements of the geminate recombination kinetics (fast pathway) or bimolecular recombination kinetics (slow pathway) at different temperatures, viscosities, pHs, and with various mutants. [43–51,58–64] Although it has been well-recognized that there are several intermediate states separated by activation barriers along the escape pathway, the CO escape process in solution at physiological temperatures has been less clear because it is spectroscopically almost silent. [78]

Advances in spectroscopic methods such as femtosecond and nanosecond time-resolved UV-visible [79,80] and IR spectroscopy [81–83] have made it possible to study the re-binding process of the photolyzed MbCO and to resolve ligand escape from the protein in real time. Based on IR spectroscopy, it was concluded that upon photodissociation of MbCO, CO becomes trapped in a docking site in the vicinity of the heme iron within a distance of a few Angströms. [45] The docking site forces CO to orient approximately parallel to the plane of the heme, which is almost perpendicular to the bound CO. This orientation and interaction in the docking site have the effect of dramatically slowing the rate of CO rebinding. The Mb docking site therefore facilitates efficient expulsion of CO from the protein with less than 2% geminate rebinding at 32 ºC. Similarly, nanosecond transient absorption spectroscopy at room temperature shows that, after photolysis of the carbon monoxide complex, about 4% of the photodissociated carbon monoxide molecules rebinds to the heme with a relaxation time of 180 ns. [45]

It is worth mentioning that these absorption spectroscopic studies only focused on structural changes around the heme chromophore and no other part of the pocket in the vicinity of the heme. Laser-induced transient grating (TG) and laser-induced photoacoustic calorimetric techniques could determine quantitatively the energetics and structural volume changes of the protein after photodissociation of MbCO and provide more detailed information about the protein dynamics during photodissociation. [84] Based on the transient grating (TG) experiments for sperm whale MbCO, the rate of ligand escape to the solvent was measured to be 700 ns at 20 °C. This fact that ligand escape is slower than the apparent geminate recombination (180 ns) clearly indicates that there is a ligand trapping site inside the protein (Figure 2.7). It should be noted that for horse heart MbCO a faster kinetics (79 ns at 20 °C) besides the 700-ns dynamics were obtained and this component might represent the CO transport process inside the protein. [84]

The photodissociation reaction scheme is shown in Figure 2.10.

In the first step, MbCO is photoexcited to the electronic excited state, where the ligand photodissociates from the heme within 2 ps; in this step, CO is trapped in the heme pocket in close proximity to the heme (Mb:CO) as the first intermediate species which can recombine and re-establish the initial Fe-CO bond. The explanation for the initial structural and enthalpy changes (t <10 ns) could be the initial movement of the proximal His and the motion of the heme. The energy of the first intermediate species (ΔH_f = 61 kJ/mol) demonstrated in Figure 2.10, is smaller than the Fe-CO bond enthalpy (105 kJ/mol). This difference indicates that the protein structure is relaxed

and stabilized after the CO dissociation within 10 ns, which is consistent with a negative volume change in the initial step (ΔV_f = -5 ml/mol).

Then, with a lifetime of 180 ns, CO goes to another trapped site where it is far enough from the heme (Mb::CO) so that it cannot recombine again. The 180 ns step is probably related to the diffusion of the CO out of the heme pocket which is accompanied by a change in the electronic state of the heme. The transfer of the CO to another site in the protein matrix does not change the protein structure significantly and could involve only a small change in enthalpy and volume and the TG signal is not sensitive enough to detect these changes. The third step is the diffusion of CO out of the protein into the solvent by a monoexponential process with a characteristic time of 700 ns at room temperature.
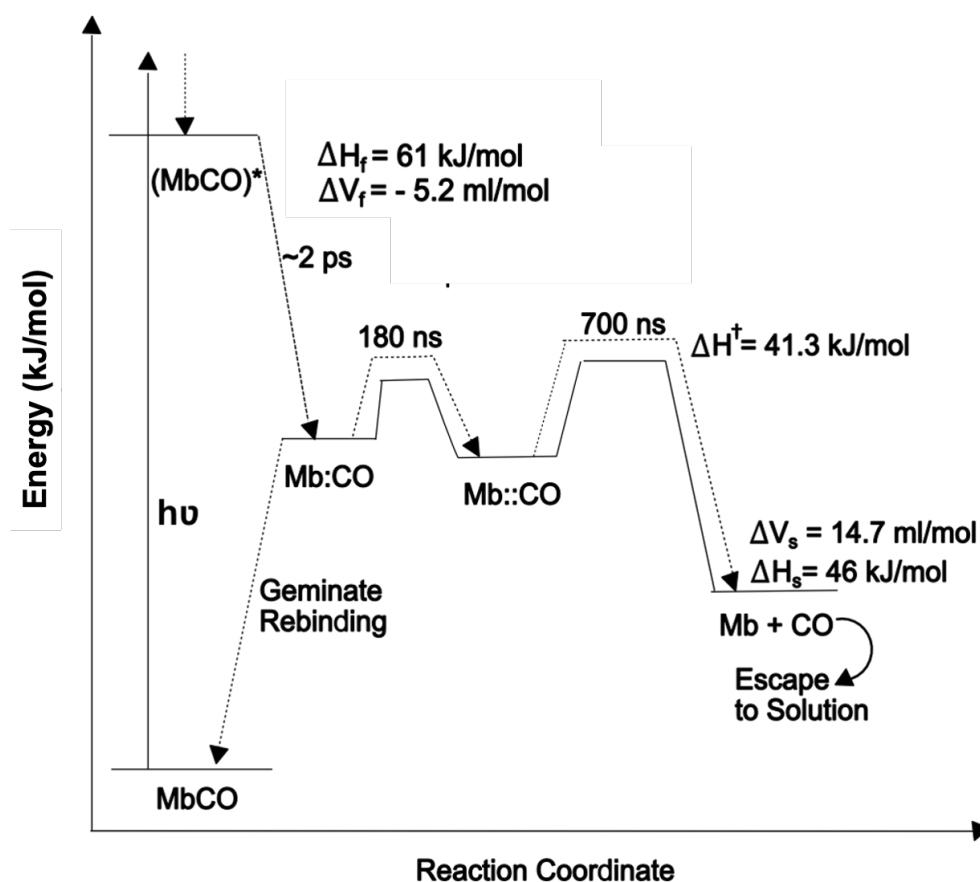
Figure 2.10. *Photodissociation reaction scheme of CO from MbCO at room temperature. After photoexcitation to the electronic excited state of MbCO, the ligand photodissociates from the heme within 2 ps; the ligand is thereby trapped in the heme pocket, and from there the CO can recombine to the heme again. On a time scale of 180 ns, the CO moves to another trapped site from which it cannot recombine to the heme. The ligand escapes from the protein to the solvent in 700 ns at room temperature. The kinetics can be expressed by a single-exponential function (modified after* [84]*).*

As demonstrated in Figure 2.10, after the initial volume contraction associated with MbCO to Mb::CO, an expansion of volume (ΔV_f = 14.7 mL/mol at 20 °C) and exothermic enthalpy changes (from $\Delta H^{\dagger}$ = 41.3 kJ/mol to ΔH_s = 46 kJ/mol) have been observed in the 700 ns step. This large effect could be explained in terms of the CO

escaping from the myoglobin into the solvent. It should be noted that this 700 ns process has not been detected by IR absorption and Raman scattering because the heme is not affected by this step.

2.7 Photodissociation at low temperature

At low temperatures, after a photoflash, the same ligand previously bound to the heme may recombine again with that heme. In contrast to the familiar exponential kinetics of elementary unimolecular reactions, below 180 K rebinding occurs nonexponentially in a 75% glycerol/water solvent. [85] It is assumed that in frozen samples (low temperature) each Mb molecule has a determined conformational state whereas, in a liquid sample (high temperature), the conformational state of each Mb molecule can change rapidly from one state to another. If, at low temperatures, the rate of transition between such conformations is slow, contrary to high temperature, each molecule will not be able to average the activation barrier over all conformations, resulting in a distribution of barrier heights instead of a sharp activation energy. [73–77,85]

2.7.1 Model for photodissociation at low temperature

Hans Frauenfelder was born on June 28, 1922,[86-87] whose 100th birthday is the occasion of this thesis, was the first who explained the structural heterogeneity of proteins using the energy landscapes. [87] An energy landscape is a map of possible atomic motions in a molecule and their related Gibbs free energy. The hypersurface of energy landscape constitutes some valleys and the free-energy minimum is related to the initial and final state of a reaction named a "state", whereas the saddle point between two minima named "transition state". Each state contains a huge number of conformational substates that hierarchally ordered into different tiers of energy (Figure 2.11).

Frauenfelder and coworkers proposed a hierarchical arrangement of conformational substates based on the photodissociation experiments on MbCO. MbCO has the conformational energy (E_c) with the unique energy valley (Figure 2.11A), which has a few taxonomic substates, exist on the highest level, denoted Tier 0 (Figure 2.11B). These substates present the energy minima separated by high free-energy barriers and they are characterized based on their structural, spectroscopic and energetic properties. For example, there are at least three substate of A_0, A_1, and A_3 (Tier 0), after photodissociation of MbCO at low temperature (T< k). They have the same primary amino acid sequence but differ, at least, in the geometry of the bound CO as shown in Figure 2.11 B at right. It should be noted that each substrate binds to CO with different rates for example, A_3 shows the slowest CO binding rate and A_0 has the fastest rate and all three substates (A_0, A_1, and A_3) rebind nonexponentially in time (Figure 2.11, right). The relative energies, entropies, and volumes for each of these substates are known and characterized. Each taxonomic substate harbors a large number of statistical substates of lower tiers such as tier 1, tier 2, teir 3,… that are separated by smaller energy barriers (Figure 2.11C). The energy landscape is changed by environmental conditions of the protein such as solvent properties, ligand binding which make it possible for protein to perform its functions. [88]
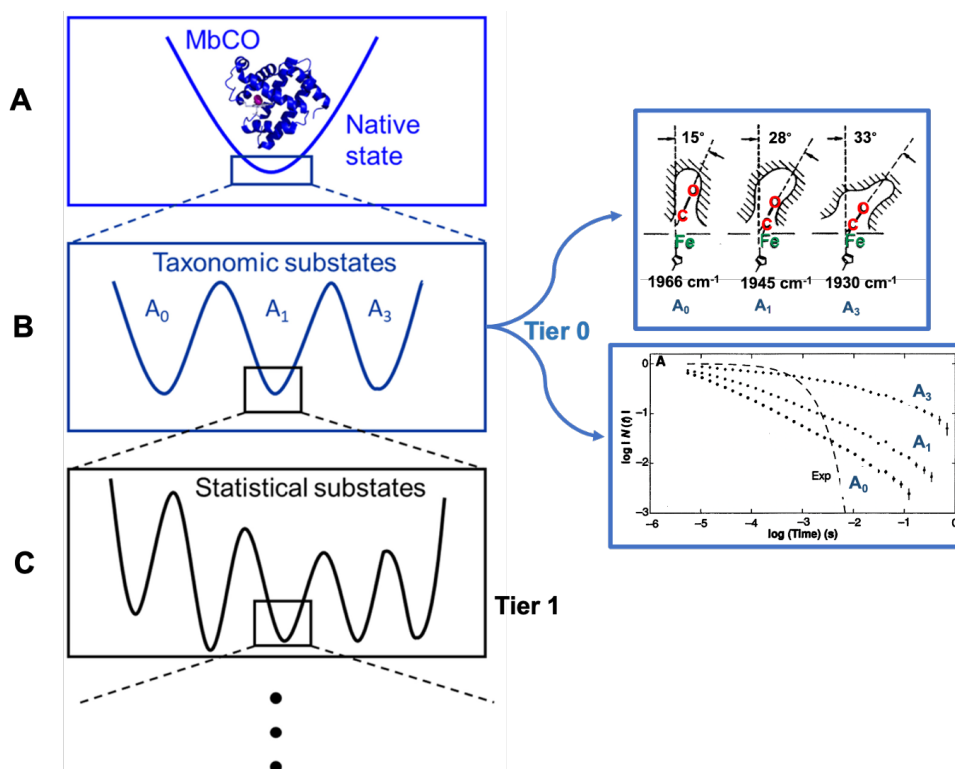
Figure 2.11 *Structure and conformational energy landscape of MbCO. The energy landscape is arranged hierarchically, with conformations nested in several tiers, according to the barriers separating the states. (A) The 3D structure of MbCO and an overall picture of the conformational energy E_c with the unique energy valley (B) (left) Three substates of Tier 0 : A_0, A_1, and A_3. (B) (right, at top) These three are due to the different orientation of the bound CO with respect to the heme, which make the different stretch band (Fe-CO). (B) (right, at down) Rebinding of CO to Mb after photodissociation, for the substates of tier 0 at pH 5.7, N(t) is the fraction of protein that have not rebound a CO at the time t after photodissociation. All three substates (A0, A1, and A3) rebind nonexponentially in time. (C) Tier 1 is vastly oversimplified. In reality, the potential energy E_c of the protein as a function of conformational coordinate is a hypersurface in a conformational space of very high dimensions and the number of valleys is extremely large. Valleys and barriers can no longer be characterized individually but must be described by distributions. [Modified after [88,89]]*

At low temperature, the protein is frozen and the CO cannot escape the protein. As the protein begin to relax (at T> 180 K), the CO can move through the different protein internal cavity. At low temperature, in photodissociation a ligand molecule bound to the iron atom undergoes a series of steps to move finally to the outside of protein by thermally overcoming all barriers. Based on research by Frauenfelder, [90] a model consisting of four steps has been proposed for low-temperature photodissociation of MbCO.

In 1991, Steinbach and coworkers defined a dynamic three-well model. This model consists of three states: The bound state (A), the pocket state (B), and the solvent state (S) (Figure 2.12). When a photon breaks the Fe-CO bond, the system moves

from A state (Fe-CO bond) to the state B. From there, the CO can either rebind directly (process I, B→A) or move to the solvent and from there bind (process S, S →B →A). Based on the experimental data of MbCO photodissociation, the process (I) has shown a temperature dependence: With increasing temperature it becomes faster up to about 170 K, but slows down above. [89]
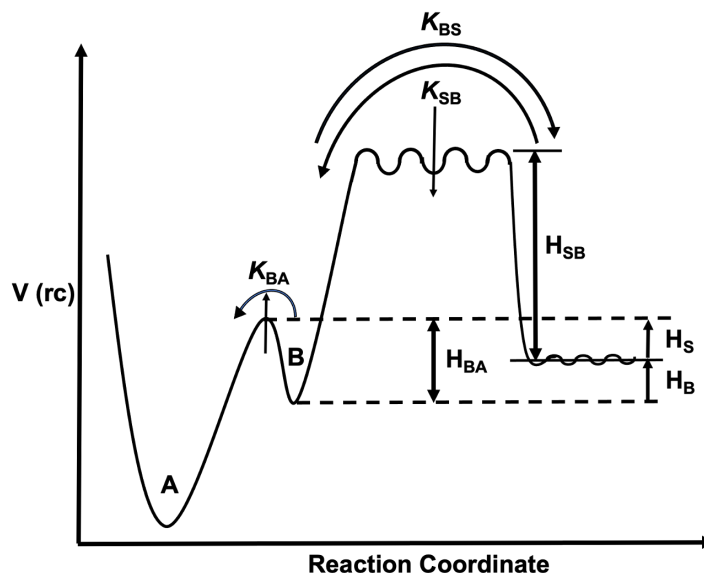
Figure 2.12 *Reaction energy landscape. The bound state, MbCO, is denoted by "A". In "B", the CO is in the heme pocket. The wiggly region demonstartes the protein matrix. "S" is the solvent.* [89]

The binding of the CO ligand to Mb is governed by the two energy barriers (Figure 2.12). The inner barrier is located at the heme iron. At temperature below 160 K in 75% glycerol, all of the large protein motions are frozen, therefore, the CO ligand cannot escape to the solvent ($\kappa_{SB} \sim 0$). After flash photolysis (T< 160 K), the rebinding of the CO to the Mb can be described by a temperature-independent distribution of enthalpic barriers g(H_{BA}). The rate coefficient $\kappa_{BA}(T)$ satisfies an Arrhenius equation that is independent of the solvent viscosity.

Between 160 K and 210 K, the protein is no longer frozen, therefore the structure of the low-temperature photoproduct starts to relax into the deoxy-Mb structure. The Mb*→Mb relaxation results in the g(H) distribution to shift toward higher enthalpies about 10 kJ/mol. The relaxation function $\Phi^*(t,T)$ is nonexponential in time based on the following equation:

$$\Phi(t,T) = e^{(-[k(T)t]^\beta)} \qquad 2.1$$

where $k(T)$ is a rate coefficient and the value of the Kohlrausch-Williams-Watts exponent β is between 0 and 1. Based on the experiments in many systems, β is essentially temperature independent over a wide range.

Moreover, the relaxation function $\Phi^*(t,T)$ is non-Arrhenius in temperature (eq. 2.2) and essentially independent of the solvent viscosity

$$\kappa(T) = A \, e^{(-\frac{E}{RT})^2} \qquad 2.2$$

When temperature rises to above 210 K, due to the equilibrium fluctuations, the CO ligand escapes into solvent on the time scale of rebinding. The transitions between the solvent S and the heme pocket B (S↔B) is formed by the fluctuations in the protein matrix. The $\kappa_1(T)$ for these equilibrium fluctuations (E$_{F1}$) shows a non-Arrhenius temperature dependence that depends strongly on the viscosity. At temperatures between 210 and 250 K and/or high solvent viscosity, the ligand binding kinetics is dominated by the outer barrier (between the solvent S and the heme pocket B). At room temperature the barrier H$_{BA}$ is still distributed, but equilibrium fluctuations (E$_{FI}$) result in average rate coefficients (κ_{BA}).

In a flash photolysis experiment on the sperm whale MbCO sample with a pulse laser (480 nm), the bond between the CO and the heme iron is broken. Experiments on band (III), a charge-transfer band at 760 nm (213000 cm^{-1}) in deoxy-Mb (the photolyzed sate of MbCO) which is absent in the bound form (MbCO). The difference in the absorption spectra at a selected wavelength, $\Delta a(t)$, for the bound and the dissociated species monitors the subsequent CO rebinding. The survival probability, $N(t,T) \equiv \Delta a(t) /\Delta a(0)$, is the fraction of Mb molecules at temperature T that have not rebound CO at the time t after the flash photolysis. The CO rebinding data to sperm whale myoglobin are shown in Figure 2.13. The faster process seen at all temperatures I for "internal"; it is nonexponential in time and independent of CO concentration. The slower process that appears above 200 K, denoted by S for "solvent", is exponential in time with a rate coefficient proportional to the CO concentration in the solvent. [89]
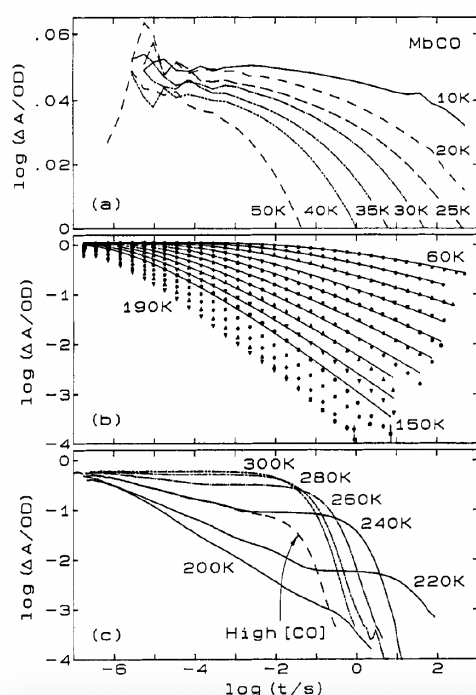
Figure 2.13 *Rebinding of CO to Mb after flash photolysis. $\Delta a(t)$, the absorbance change at the time t after photodissociation, measured at 440 nm, is plotted versus log t. $\Delta a(0)$ = 1.12 OD below 200 K, pH 6.8. Solvent: 75% glycerol/buffer (v/v). CO pressure in (c): 1 bar for the high-[CO] curve and 0.05 bar for the solid curves. Note that the scale in panel a is expanded by a factor of approximately 100. [89]*

In conclusion, the association coefficient for binding CO from the solvent at physiological temperatures to Mb is governed by the barrier at the heme. At low temperature, the CO rebinding rate depends on the conformational substate, which exhibit rate fluctuations, and make a non-exponential kinetics and heterogeneity of protein dynamics.

2.8 Outline

Myoglobin (Mb) has been used over decays as a model system for many experimental and theoretical studies particularly for kinetics-structural relationships. The heme, as a reaction center, is embedded within the protein and small ligands such as O_2, CO, or NO can reversibly and covalently bind to the sixth coordination site on the distal side, of the heme. The binding and rebinding rate of such small molecules, for example CO, to the heme varies with temperature, pH, mutant, etc. and yield a lot of information about how structure, dynamics, and reactivity correlate to the environment conditions. [43–51,58–64]

Low-temperature experiments by Frauenfelder and coworkers in the 1970s demonstrated that, at cryogenic temperatures, rebinding of CO to myoglobin's heme cofactor after flash photolysis shows a strongly stretched exponential behavior, which is not observed at room temperature. [69–72,84,87,90] This behavior has been assigned to structural heterogeneity of myoglobin, resulting in different rebinding rates of CO, but no direct observation of this effect exists to date.

In recent years, the single-molecule methods for studying the kinetic behavior of individual molecular complexes have been developed in particular to determine heterogeneous behaviors in a system. [91-92] Moreover, dynamic heterogeneity, i.e. the dynamic switching of a protein between different states during the time of the experiment, makes it impossible to investigate an individual molecular dynamics in an ensemble measurement because may yield an average value for the experimental observables. Therefore, reducing the observed "ensemble" to a single molecule immediately solves the above-mentioned problems and make it possible to look individually the characteristics of each single molecule. Now, subpopulations can be easily resolved and also dynamic switching between different states can be observed. Recently, a new effort to take advantage of Förster Resonance Energy Transfer (FRET) technology to determine protein interaction and binding-rebinding reaction has emerged. In this approach, the donor emission is quenched through a non-fluorescent acceptor (protein) that can be used to study protein rebinding kinetics. [93] The method using quenched donor emission has more general applications as the acceptor can be a different state of myoglobin with different quenching effects for example deoxy-Mb, in which the CO is unbound to Mb, can act as a quencher and MbCO, where the CO is bound to Mb, has no quenching effects, or less. The binding and rebinding of diatomic molecules such as NO, and CO to the heme proteins have been studied through the change in the absorption of band III. [94]

The rebinding kinetics of CO can be measured precisely through quenching of a fluorescent dye attached to the myoglobin protein using FRET. Selection of the proper dye, position of labeling on the protein and the labelling method are crucial. For this purpose, not only an independent estimation of the FRET efficiency is needed to characterize protein re-binding but also the development of quantitative methodologies for steady-state and kinetic parameters of protein binding to the ligand is crucial. In the beginning of chapter 4, we focus on two different labelling methods,

different dye and different labeling sites on myoglobin. In the second part of Chapter 4, FRET experiments on dye-labelled Met-Mb, Deoxy-Mb and MbCO are reported. Chapter 4 describes ensemble FRET experiments of dye labeled -MbCO that demonstrate the feasibility of performing single molecule-FRET experiments.

Blue light breaks the Mb-CO bond with an efficiency of unity, which precludes FRET-based investigations of Mb-CO, as the bond between heme and CO would break after FRET. It means that before the carbonoxy state can be measured it has been already converted to the deoxy form. Therefore, the main question to be answered is whether the light emitted by the label can break the Mb-CO bond (due to the FRET) and with what efficiency it. Chapter 3 is about answering this question and proposing a new approach for the possibility of a FRET study of dye-labeled MbCO.

As discussed in Chapter 2, the myoglobin spectrum can be broadly split into three parts: the Soret band (300-500 nm), the Q-bands (500-700 nm) and the NIR bands (700-1000 nm). The quantum yield of breaking the Mb-CO bond is unity when it is illuminated by light with wavelengths below 600 nm. However, it is still unknown if illumination with light with a wavelength longer than 600 nm in particularly in the far red range breaks the MbCO bond or not and what its quantum yield would be?

In chapter 3, we describe experiments to determine the quantum yield of dissociation under far red illumination in order to determine if that region can be used for the FRET experiments.

In chapter 3, we propose an approach using the weak bands beyond 700 nm in the deoxy-Mb absorption spectrum to quench the fluorescence of a deep red dye. Crucially, these bands are absent in the spectrum of MbCO, preventing breakage of the CO bond due to resonant energy transfer from the excited dye. As the different states of Mb can be readily distinguished by their UV/Vis spectra, this method was selected to determine the dissociation quantum yield. To study photodissociation kinetics of MbCO, firstly Mb-CO was illuminated by near infra-red LED light. Then, following the absorption spectrum over time after each illumination cycle, we measure the kinetics of Mb-CO bond breaking. This experiment is repeated for blue light as a reference and the kinetics were compared.

The aim of Chapter 3 and 4 is to show the rebinding of CO to a protein at the single-molecule level can be done by performing single molecule-FRET experiments.

The histogram of FRET efficiencies and the corresponding donor-acceptor distances extracted from single-pair FRET data make it possible to follow the structural dynamics of biomolecules over time, and to distinguish the different surrounding environments of single molecules. However, in ensemble experiments, both the spatial and temporal heterogeneities are averaged out, and most of the information about the complexity of the system is lost. Therefore, in chapter 5, we study the FRET quenching in a system with a distribution of acceptors (ATTO575Q dye) around the donor (Azaoxa-triangulenium, ADOTA dye) dopped in thin polymeric layers at both ensemble and single molecule level at room temperature to measure and prove these heterogeneities in single molecule level which are averaged out in the ensemble.

References

(1) Wittenberg, B. A.; Wittenberg, J. B. Myoglobin-Mediated Oxygen Delivery to Mitochondria of Isolated Cardiac Myocytes. *Proc. Natl. Acad. Sci. U. S. A.* **1987**, *84* (21), 7503–7507.

(2) Gros, G.; Wittenberg, B. A.; Jue, T. Myoglobin's Old and New Clothes: From Molecular Structure to Function in Living Cells. *J. Exp. Biol.* **2010**, *213* (16), 2713–2725.

(3) Wittenberg, B. A.; Wittenberg, J. B. Transport of Oxygen in Muscle. *Annu. Rev. Physiol.* **1989**, *51*, 857–878.

(4) Gomez-Cambronero, J. THE OXYGEN DISSOCIATION CURVE OF HEMOGLOBIN: BRIDGING THE GAP BETWEEN BIOCHEMISTRY AND PHYSIOLOGY. *J. Chem. Educ.* **2001**, *78* (6), 757.

(5) Antonini, E. INTERRELATIONSHIP BETWEEN STRUCTURE AND FUNCTION IN HEMOGLOBIN AND MYOGLOBIN. *Physiol. Rev.* **1965**, *45*, 123–170.

(6) Hemoglobin and Myoglobin | Integrative Medical Biochemistry Examination and Board Review | AccessPharmacy | McGraw Hill Medical https://accesspharmacy.mhmedical.com/content.aspx?bookid=1696&sectionid=111398218 (accessed 2022 -01 -14).

(7) Ryter, S. W.; Otterbein, L. E. Carbon Monoxide in Biology and Medicine. *BioEssays News Rev. Mol. Cell. Dev. Biol.* **2004**, *26* (3), 270–280.

(8) Liu, Z.; Meng, H.; Huang, J.; Kwangwari, P.; Ma, K.; Xiao, B.; Li, L. Acute Carbon Monoxide Poisoning with Low Saturation of Carboxyhaemoglobin: A Forensic Retrospective Study in Shanghai, China. *Sci. Rep.* **2021**, *11* (1), 18554.

(9) Bleecker, M. L. Carbon Monoxide Intoxication. *Handb. Clin. Neurol.* **2015**, *131*, 191–203.

(10) Miró, O.; Casademont, J.; Barrientos, A.; Urbano-Márquez, A.; Cardellach, F. Mitochondrial Cytochrome c Oxidase Inhibition during Acute Carbon Monoxide Poisoning. *Pharmacol. Toxicol.* **1998**, *82* (4), 199–202.

(11) Kim, H. P.; Ryter, S. W.; Choi, A. M. K. CO as a Cellular Signaling Molecule. *Annu. Rev. Pharmacol. Toxicol.* **2006**, *46*, 411–449.

(12) Boehning, D.; Snyder, S. H. Circadian Rhythms. Carbon Monoxide and Clocks. *Science* **2002**, *298* (5602), 2339–2340.

(13) Kobayashi, A.; Ishikawa, K.; Matsumoto, H.; Kimura, S.; Kamiyama, Y.; Maruyama, Y. Synergetic Antioxidant and Vasodilatory Action of Carbon Monoxide in Angiotensin II - Induced Cardiac Hypertrophy. *Hypertens. Dallas Tex 1979* **2007**, *50* (6), 1040–1048.

(14) Kendrew, J. C.; Bodo, G.; Dintzis, H. M.; Parrish, R. G.; Wyckoff, H.; Phillips, D. C. A Three-Dimensional Model of the Myoglobin Molecule Obtained by x-Ray Analysis. *Nature* **1958**, *181* (4610), 662–666.

(15) Ordway, G. A.; Garry, D. J. Myoglobin: An Essential Hemoprotein in Striated Muscle. *J. Exp. Biol.* **2004**, *207* (Pt 20), 3441–3446.

(16) Fleischer, E. B. Structure of Porphyrins and Metalloporphyrins. *Acc. Chem. Res.* **1970**, *3* (3), 105–112.

(17) Porphyrin. *Wikipedia*; 2022.

(18) Dolphin, D. *The Porphyrins V3: Physical Chemistry, Part A*; Elsevier, 2012.

(19) Goldoni, A. Porphyrins: Fascinating Molecules with Biological Significance.

(20) Eaton, W. A.; Hanson, L. K.; Stephens, P. J.; Sutherland, J. C.; Dunn, J. B. R. Optical Spectra of Oxy- and Deoxyhemoglobin. *J. Am. Chem. Soc.* **1978**, *100* (16), 4991–5003.

(21) Bowen, W. J. The Absorption Spectra and Extinction Coefficients of Myoglobin. *J. Biol. Chem.* **1949**, *179* (1), 235–245.

(22) Namuangruk, S.; Sirithip, K.; Rattanawan, R.; Keawin, T.; Kungwan, N.; Sudyodsuk, T.; Promarak, V.; Surakhot, Y.; Jungsuttiwong, S. Theoretical Investigation of the Charge-Transfer Properties in Different Meso-Linked Zinc Porphyrins for Highly Efficient Dye-Sensitized Solar Cells. *Dalton Trans. Camb. Engl. 2003* **2014**, *43*.

(23) Gouterman, M. Spectra of Porphyrins. *J. Mol. Spectrosc.* **1961**, *6*, 138–163.

(24) Uddin, J. *Macro To Nano Spectroscopy*; BoD – Books on Demand, 2012.

(25) Kingsbury, C. J.; Senge, M. O. The Shape of Porphyrins. *Coord. Chem. Rev.* **2021**, *431*, 213760.

(26) Cupane, A.; Leone, M.; Vitrano, E.; Cordone, L. Structural and Dynamic Properties of the Heme Pocket in Myoglobin Probed by Optical Spectroscopy. *Biopolymers* **1988**, *27* (12), 1977–1997.

(27) Franzen, S.; Wallace-Williams, S. E.; Shreve, A. P. Heme Charge-Transfer Band III Is Vibronically Coupled to the Soret Band. *J. Am. Chem. Soc.* **2002**, *124* (24), 7146–7155.

(28) Cordone, L.; Cupane, A.; Leone, M.; Vitrano, E. Thermal Behavior of the 760-Nm Absorption Band in Photodissociated Sperm Whale Carbonmonoxymyoglobin at Cryogenic Temperature: Dependence on External Medium. *Biopolymers* **1990**, *29* (3), 639–643.

(29) Sharonov, Y. A.; Sharonova, N. A.; Figlovsky, V. A.; Grigorjev, V. A. A Comparison of the Heme Electronic States in Equilibrium and Nonequilibrium Protein Conformations of High-Spin Ferrous Hemoproteins Low Temperature Magnetic Circular Dichroism Studies. *Biochim. Biophys. Acta BBA - Protein Struct. Mol. Enzymol.* **1982**, *709* (2), 332–341.

(30) Makinen, M. W.; Houtchens, R. A.; Caughey, W. S. Structure of Carboxymyoglobin in Crystals and in Solution. *Proc. Natl. Acad. Sci. U. S. A.* **1979**, *76* (12), 6042–6046.

(31) Chance, B.; Lee, C.; Blasie, J. K. *Probes and Membrane Function*; Academic Press, 2013.

(32) Olson, J. S.; Soman, J.; Phillips, G. N. Ligand Pathways in Myoglobin: A Review of Trp Cavity Mutations. *IUBMB Life* **2007**, *59* (8–9), 552–562.

(33) Vos, M. H. Ultrafast Dynamics of Ligands within Heme Proteins. *Biochim. Biophys. Acta BBA - Bioenerg.* **2008**, *1777* (1), 15–31.

(34) Shelby, M. L.; Wildman, A.; Hayes, D.; Mara, M. W.; Lestrange, P. J.; Cammarata, M.; Balducci, L.; Artamonov, M.; Lemke, H. T.; Zhu, D.; Seideman, T.; Hoffman, B. M.; Li, X.; Chen, L. X. Interplays of Electron and Nuclear Motions along CO Dissociation Trajectory in Myoglobin Revealed by Ultrafast X-Rays and Quantum Dynamics Calculations. *Proc. Natl. Acad. Sci.* **2021**, *118* (14), e2018966118.

(35) Ionascu, D.; Gruia, F.; Ye, X.; Yu, A.; Rosca, F.; Beck, C.; Demidov, A.; Olson, J. S.; Champion, P. M. Temperature-Dependent Studies of NO Recombination to Heme and Heme Proteins. *J. Am. Chem. Soc.* **2005**, *127* (48), 16921–16934.

(36) Sakakura, M.; Yamaguchi, S.; Hirota, N.; Terazima, M. Dynamics of Structure and Energy of Horse Carboxymyoglobin after Photodissociation of Carbon Monoxide. *J. Am. Chem. Soc.* **2001**, *123* (18), 4286–4294.

(37) Sakakura, M.; Morishima, I.; Terazima, M. The Structural Dynamics and Ligand Releasing Process after the Photodissociation of Sperm Whale Carboxymyoglobin. *J. Phys. Chem. B* **2001**, *105* (42), 10424–10434.

(38) Waleh, A.; Loew, G. H. Quantum Mechanical Studies of the Photodissociation of Carbonylheme Complexes. *J. Am. Chem. Soc.* **1982**, *104* (9), 2346–2351.

(39) Barends, T. R. M.; Foucar, L.; Ardevol, A.; Nass, K.; Aquila, A.; Botha, S.; Doak, R. B.; Falahati, K.; Hartmann, E.; Hilpert, M.; Heinz, M.; Hoffmann, M. C.; Köfinger, J.; Koglin, J. E.; Kovacsova, G.; Liang, M.; Milathianaki, D.; Lemke, H. T.; Reinstein, J.; Roome, C. M.; Shoeman, R. L.; Williams, G. J.; Burghardt, I.; Hummer, G.; Boutet, S.; Schlichting, I. Direct Observation of Ultrafast Collective Motions in CO Myoglobin upon Ligand Dissociation. *Science* **2015**, *350* (6259), 445–450.

(40) Harvey, J. N. DFT Computation of the Intrinsic Barrier to CO Geminate Recombination with Heme Compounds. *J. Am. Chem. Soc.* **2000**, *122* (49), 12401–12402.

(41) Harvey, J. N. Spin-Forbidden CO Ligand Recombination in Myoglobin. *Faraday Discuss.* **2004**, *127* (0), 165–177.

(42) Dunietz, B. D.; Dreuw, A.; Head-Gordon, M. Initial Steps of the Photodissociation of the CO Ligated Heme Group. *J. Phys. Chem. B* **2003**, *107* (23), 5623–5629.

(43) Petrich, J. W.; Poyart, C.; Martin, J. L. Photophysics and Reactivity of Heme Proteins: A Femtosecond Absorption Study of Hemoglobin, Myoglobin, and Protoheme. *Biochemistry* **1988**, *27* (11), 4049–4060.

(44) Srajer, V.; Teng, T.; Ursby, T.; Pradervand, C.; Ren, Z.; Adachi, S.; Schildkamp, W.; Bourgeois, D.; Wulff, M.; Moffat, K. Photolysis of the Carbon Monoxide Complex of Myoglobin: Nanosecond Time-Resolved Crystallography. *Science* **1996**, *274* (5293), 1726–1729.

(45) Henry, E. R.; Sommer, J. H.; Hofrichter, J.; Eaton, W. A. Geminate Recombination of Carbon Monoxide to Myoglobin. *J. Mol. Biol.* **1983**, *166* (3), 443–451.

(46) Levantino, M.; Schirò, G.; Lemke, H. T.; Cottone, G.; Glownia, J. M.; Zhu, D.; Chollet, M.; Ihee, H.; Cupane, A.; Cammarata, M. Ultrafast Myoglobin Structural Dynamics Observed with an X-Ray Free-Electron Laser. *Nat. Commun.* **2015**, *6* (1), 6772.

(47) Levantino, M.; Lemke, H. T.; Schirò, G.; Glownia, M.; Cupane, A.; Cammarata, M. Observing Heme Doming in Myoglobin with Femtosecond X-Ray Absorption Spectroscopy. *Struct. Dyn.* **2015**, *2* (4), 041713.

(48) Dartigalongue, T.; Hache, F. Observation of Sub-100 Ps Conformational Changes in Photolyzed Carbonmonoxy-Myoglobin Probed by Time-Resolved Circular Dichroism. In *11th Congress of the European Society for Photobiology*; oral; Aix les Bains, France, 2005.

(49) Findsen, E. W.; Scott, T. W.; Chance, M. R.; Friedman, J. M.; Ondrias, M. R. Picosecond Time-Resolved Raman Studies of Photodissociated Carboxymyoglobin. *J. Am. Chem. Soc.* **1985**, *107* (11), 3355–3357.

(50) Ferrante, C.; Pontecorvo, E.; Cerullo, G.; Vos, M. H.; Scopigno, T. Direct Observation of Subpicosecond Vibrational Dynamics in Photoexcited Myoglobin. *Nat. Chem.* **2016**, *8* (12), 1137–1143.

(51) Franzen, S.; Bohn, B.; Poyart, C.; Martin, J. L. Evidence for Sub-Picosecond Heme Doming in Hemoglobin and Myoglobin: A Time-Resolved Resonance Raman Comparison of Carbonmonoxy and Deoxy Species. *Biochemistry* **1995**, *34* (4), 1224–1237.

(52) Ostermann, A.; Waschipky, R.; Parak, F. G.; Nienhaus, G. U. Ligand Binding and Conformational Motions in Myoglobin. *Nature* **2000**, *404* (6774), 205–208.

(53) Schoenborn, B. P.; Watson, H. C.; Kendrew, J. C. Binding of Xenon to Sperm Whale Myoglobin. *Nature* **1965**, *207* (4992), 28–30.

(54) Bossa, C.; Anselmi, M.; Roccatano, D.; Amadei, A.; Vallone, B.; Brunori, M.; Di Nola, A. Extended Molecular Dynamics Simulation of the Carbon Monoxide Migration in Sperm Whale Myoglobin. *Biophys. J.* **2004**, *86* (6), 3855–3862.

(55) Schmidt, M.; Nienhaus, K.; Pahl, R.; Krasselt, A.; Anderson, S.; Parak, F.; Nienhaus, G. U.; Šrajer, V. Ligand Migration Pathway and Protein Dynamics in

Myoglobin: A Time-Resolved Crystallographic Study on L29W MbCO. *Proc. Natl. Acad. Sci.* **2005**, *102* (33), 11704–11709.

(56) Samuni, U.; Dantsker, D.; Roche, C. J.; Friedman, J. M. Ligand Recombination and a Hierarchy of Solvent Slaved Dynamics: The Origin of Kinetic Phases in Hemeproteins. *Gene* **2007**, *398* (1), 234–248.

(57) Falahati, K.; Tamura, H.; Burghardt, I.; Huix-Rotllant, M. Ultrafast Carbon Monoxide Photolysis and Heme Spin-Crossover in Myoglobin via Nonadiabatic Quantum Dynamics. *Nat. Commun.* **2018**, *9* (1), 4502.

(58) Murray, L. P.; Hofrichter, J.; Henry, E. R.; Eaton, W. A. Time-Resolved Optical Spectroscopy and Structural Dynamics Following Photodissociation of Carbonmonoxyhemoglobin. *Biophys. Chem.* **1988**, *29* (1–2), 63–76.

(59) Hamdane, D.; Kiger, L.; Hui-Bon-Hoa, G.; Marden, M. C. Kinetics inside the Protein: Shape of the Geminate Kinetics in Myoglobin. *J. Phys. Chem. B* **2011**, *115* (14), 3919–3923.

(60) Kleinert, T.; Doster, W.; Leyser, H.; Petry, W.; Schwarz, V.; Settles, M. Solvent Composition and Viscosity Effects on the Kinetics of CO Binding to Horse Myoglobin. *Biochemistry* **1998**, *37* (2), 717–733. https://doi.org/10.1021/bi971508q.

(61) Angeloni, L.; Feis, A. Protein Relaxation in the Photodissociation of Myoglobin–CO Complexes. *Photochem. Photobiol. Sci.* **2003**, *2* (7), 730–740.

(62) Ansari, A.; Jones, C. M.; Henry, E. R.; Hofrichter, J.; Eaton, W. A. Conformational Relaxation and Ligand Binding in Myoglobin. *Biochemistry* **1994**, *33* (17), 5128–5145.

(63) Jongeward, K. A.; Magde, Douglas.; Taube, D. J.; Marsters, J. C.; Traylor, T. G.; Sharma, V. S. Picosecond and Nanosecond Geminate Recombination of Myoglobin with Carbon Monoxide, Oxygen, Nitric Oxide and Isocyanides. *J. Am. Chem. Soc.* **1988**, *110* (2), 380–387.

(64) Dartigalongue, T.; Niezborala, C.; Hache, F. Subpicosecond UV Spectroscopy of Carbonmonoxy-Myoglobin: Absorption and Circular Dichroism Studies. *Phys. Chem. Chem. Phys. PCCP* **2007**, *9*, 1611–1615.

(65) Schmidt, M.; Nienhaus, K.; Pahl, R.; Krasselt, A.; Anderson, S.; Parak, F.; Nienhaus, G. U.; Srajer, V. Ligand Migration Pathway and Protein Dynamics in Myoglobin: A Time-Resolved Crystallographic Study on L29W MbCO. *Proc. Natl. Acad. Sci. U. S. A.* **2005**, *102* (33), 11704–11709.

(66) Maragliano, L.; Cottone, G.; Ciccotti, G.; Vanden-Eijnden, E. Mapping the Network of Pathways of CO Diffusion in Myoglobin. *J. Am. Chem. Soc.* **2010**, *132* (3), 1010–1017.

(67) Brunori, M.; Bourgeois, D.; Vallone, B. The Structural Dynamics of Myoglobin. *J. Struct. Biol.* **2004**, *147* (3), 223–234. https://doi.org/10.1016/j.jsb.2004.04.008.

(68) Tetreau, C.; Lavalette, D. Dominant Features of Protein Reaction Dynamics: Conformational Relaxation and Ligand Migration. *Biochim. Biophys. Acta BBA - Gen. Subj.* **2005**, *1724* (3), 411–424.

(69) Austin, R. H.; Beeson, K. W.; Eisenstein, L.; Frauenfelder, H.; Gunsalus, I. C. Dynamics of Ligand Binding to Myoglobin. *Biochemistry* **1975**, *14* (24), 5355–5373.

(70) Frauenfelder, H.; Wolynes, P. G.; Austin, R. H. Biological Physics. *Rev. Mod. Phys.* **1999**, *71* (2), S419–S430.

(71) Frauenfelder, H.; Wolynes, P. G. Rate Theories and Puzzles of Hemeprotein Kinetics. *Science* **1985**, *229* (4711), 337–345.

(72) Frauenfelder, H.; Sligar, S. G.; Wolynes, P. G. The Energy Landscapes and Motions of Proteins. *Science* **1991**, *254* (5038), 1598–1603.

(73) Reynolds, A. H.; Rentzepis, P. M. Kinetics and Temperature Dependence of Carboxymyoglobin Ligand Photodissociation. *Biophys. J.* **1982**, *38* (1), 15–18.

(74) Ansari, A.; Berendzen, J.; Bowne, S. F.; Frauenfelder, H.; Iben, I. E.; Sauke, T. B.; Shyamsunder, E.; Young, R. D. Protein States and Proteinquakes. *Proc. Natl. Acad. Sci.* **1985**, *82* (15), 5000–5004.

(75) Tomita, A.; Sato, T.; Nozawa, S.; Koshihara, S.; Adachi, S. Tracking Ligand-Migration Pathways of Carbonmonoxy Myoglobin in Crystals at Cryogenic Temperatures. *Acta Crystallogr. A* **2010**, *66* (Pt 2), 220–228.

(76) Tian, W. D.; Sage, J. T.; Champion, P. M.; Chien, E.; Sligar, S. G. Probing Heme Protein Conformational Equilibration Rates with Kinetic Selection. *Biochemistry* **1996**, *35* (11), 3487–3502. https://doi.org/10.1021/bi952474u.

(77) Olson, J. S.; Phillips, G. N. Kinetic Pathways and Barriers for Ligand Binding to Myoglobin. *J. Biol. Chem.* **1996**, *271* (30), 17593–17596.

(78) Nienhaus, K.; Deng, P.; Kriegl, J. M.; Nienhaus, G. U. Structural Dynamics of Myoglobin: Effect of Internal Cavities on Ligand Migration and Binding. *Biochemistry* **2003**, *42* (32), 9647–9658.

(79) Reynolds, A. H.; Rand, S. D.; Rentzepis, P. M. Mechanisms for Excited State Relaxation and Dissociation of Oxymyoglobin and Carboxymyoglobin. *Proc. Natl. Acad. Sci. U. S. A.* **1981**, *78* (4), 2292–2296.

(80) Henry, E. R.; Sommer, J. H.; Hofrichter, J.; Eaton, W. A. Geminate Recombination of Carbon Monoxide to Myoglobin. *J. Mol. Biol.* **1983**, *166* (3), 443–451.

(81) Bredenbeck, J.; Helbing, J.; Nienhaus, K.; Nienhaus, G. U.; Hamm, P. Protein Ligand Migration Mapped by Nonequilibrium 2D-IR Exchange Spectroscopy. *Proc. Natl. Acad. Sci.* **2007**, *104* (36), 14243–14248.

(82) Nienhaus, K.; Olson, J. S.; Franzen, S.; Nienhaus, G. U. The Origin of Stark Splitting in the Initial Photoproduct State of MbCO. *J. Am. Chem. Soc.* **2005**, *127* (1), 40–41.

(83) Ansari, A.; Berendzen, J.; Braunstein, D.; Cowen, B. R.; Frauenfelder, H.; Hong, M. K.; Iben, I. E.; Johnson, J. B.; Ormos, P.; Sauke, T. B. Rebinding and Relaxation in the Myoglobin Pocket. *Biophys. Chem.* **1987**, *26* (2–3), 337–355.

(84) Sakakura, M.; Yamaguchi, S.; Hirota, N.; Terazima, M. Dynamics of Structure and Energy of Horse Carboxymyoglobin after Photodissociation of Carbon Monoxide. *J. Am. Chem. Soc.* **2001**, *123* (18), 4286–4294.

(85) Agmon, N.; Hopfield, J. J. CO Binding to Heme Proteins: A Model for Barrier Height Distributions and Slow Conformational Changes. *J. Chem. Phys.* **1983**, *79* (4), 2042.

(86) https://en.wikipedia.org/wiki/Hans_Frauenfelder

(87) Frauenfelder, H.; Sligar, S. G.; Wolynes, P. G. The Energy Landscapes and Motions of Proteins. *Science, New Series, 254* (5038), 1598-1603.

(88) Manz, C.; Kobitski, A. Y.; Samanta, A., Nienhaus, K.; Jäschke, A.; Nienhaus, G. U. Exploring the energy landscape of a SAM-I riboswitch. J. Biol. Phys. **2021**, *47*, 371–386.

(89) Steinbach P. J.; Ansari, A.; Berendzen, J.; Braunstein, D.; Chu, K.; Cowen, B. R.; Ehrenstein, D.; Frauenfelder, H.; Johnson, J. B. Ligand binding to heme proteins: connection between dynamics and function. *Biochemistry* **1991**, *30* (16), 3988-4001.

(90) Austin, R. H.; Beeson, K. W.; Eisenstein, L.; Frauenfelder, H.; Gunsalus, I. C. Dynamics of Ligand Binding to Myoglobin. *Biochemistry* **1975**, *14* (24), 5355–5373.

(91) Sustarsic, M.; Kapanidis, A. N. Taking the Ruler to the Jungle: Single-Molecule FRET for Understanding Biomolecular Structure and Dynamics in Live Cells. *Curr. Opin. Struct. Biol.* **2015**, *34*, 52–59.

(92) Pradhan, B.; Engelhard, C.; Mulken, S. V.; Miao, X.; Canters, G. W.; Orrit, M. Single Electron Transfer Events and Dynamical Heterogeneity in the Small Protein Azurin from Pseudomonas Aeruginosa. *Chem. Sci.* **2020**, *11* (3), 763–771.

(93) Penjweini, R.; Andreoni, A.; Rosales, T.; Kim, J.; Brenner, M. D.; Sackett, D. L.; Chung, J. H.; Knutson, J. R. Intracellular Oxygen Mapping Using a Myoglobin-MCherry Probe with Fluorescence Lifetime Imaging. *J. Biomed. Opt.* **2018**, *23* (10), 1–14.

(94) Yoo, B.-K.; Kruglik, S. G.; Lamarre, I.; Martin, J.-L.; Negrerie, M. Absorption band III kinetics probe the picosecond heme iron motion triggered by nitric oxide binding to hemoglobin and myoglobin. *J. Phys. Chem. B* **2012** *116* (13), 4106-4114.